Full-field analysis of notch effects of 3D carbon/carbon composites

Lijun Qin, Zhongwei Zhang, Zhihai Feng, Xiaofeng Li, Yu Wang, Yang Wang, Hong Miao, Linghui He & Xinglong Gong

Journal of Materials Science
Full Set - Includes `Journal of Materials Science Letters'

ISSN 0022-2461
Volume 48
Number 9

J Mater Sci (2013) 48:3454-3460
DOI 10.1007/s10853-013-7135-x

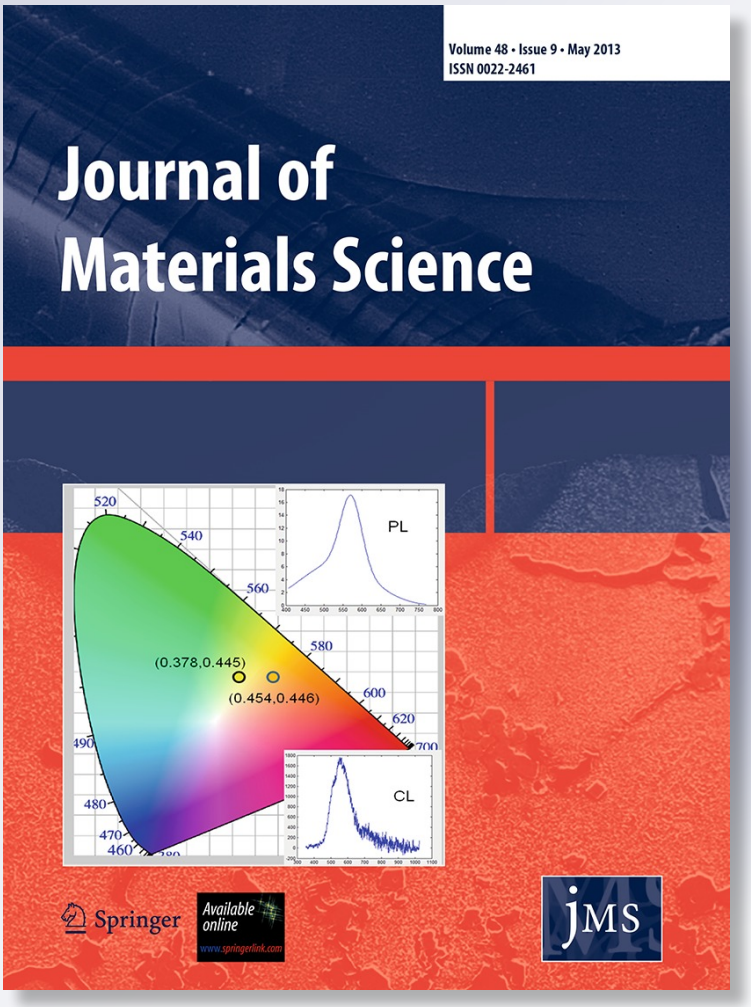

Springer

J Mater Sci (2013) 48:3454–3460
DOI 10.1007/s10853-013-7135-x

Full-field analysis of notch effects of 3D carbon/carbon composites

Lijun Qin · Zhongwei Zhang · Zhihai Feng · Xiaofeng Li · Yu Wang · Yang Wang · Hong Miao · Linghui He · Xinglong Gong

Received: 4 December 2012 / Accepted: 3 January 2013 / Published online: 9 January 2013

Abstract Carbon fiber reinforced carbon matrix composites (C/Cs), as important candidate aviation and aerospace materials, have good prospects for application in extreme environments. However, notch effects of C/Cs have not been studied adequately. In this work, the notch effects of 3D-C/C composites were investigated by the full-field measurement digital image correlation method. Six kinds of specimens with different notch patterns including one central hole, multi-holes, and double edge notches, were examined to analyze their mechanical properties. The tests were carried out on MTS 809 testing machine and the deformations of specimens were monitored by a CCD camera. Using the full-field measurement, both the local mechanical properties (stress concentration, shear damage, and fracture behavior) and the globe properties (notch sensitivity and tensile behavior) were studied. The results indicated that the fracture stress on the net cross section was constant and it was independent on the material heterogeneity, notch patterns, and notch depth.

Introduction

In aviation and aerospace applications, cutting notches and holes are common and important ways to connect different structure parts together. The notch effects, such as stress concentration, local damages, stiffness, and strength loss, are critical mechanical properties for structure designation. The notch effects of advanced materials are initially investigated in the ceramic matrix composites (CMCs) [1–5]. Three classes of stress redistribution mechanisms can lead to the excellent notched strength performance of CMCs: class I, matrix cracking and fiber failure; class II, matrix cracking; class III, shear damage by matrix cracking [2]. As important candidate aviation and aerospace materials, carbon fiber reinforced carbon matrix composites (C/Cs) have good prospects for application in extreme environments, because of their ability to sustain high modulus and high strength under elevated temperature [6–9]. However, notch effects of C/Cs have not been investigated adequately.

Recently, the notch effects of 2D-C/Cs have been systematically studied [10–13]. Kostopoulos and Pappas [11] hypothesized the existence of a damage zone in the hole tip and they considered that the stress in damage zone was equal to the unnotched strength. Based on their assumption, they successfully predicted the notched strength of 2D-C/Cs. However, later investigation showed that the fracture stress in the notch root was not always equal to the unnotched strength. Using the double edge notched (DEN) specimens, Aly-Hassan et al. [6] reported that the fracture stress was higher or lower than unnotched strength when the notch length was short or long. Another inconsistent report was the mechanism of the high notched strength of 2D-C/Cs. Griesheim et al. [13] regarded an independent damage mechanism existence to absorb energy but not to alter the ultimate fracture load. Based on their study, the candidates for the damage mechanism were fiber pull-out and shear damages. However, many other experiments showed that the mechanism of the high notched strength was not the shear damages but the zigzag cracking or the

L. Qin · X. Li · Y. Wang · Y. Wang · H. Miao · L. He · X. Gong (✉)
CAS Key Laboratory of Mechanical Behavior and Design of Materials, Department of Modern Mechanics, University of Science and Technology of China, Hefei 230027, China
e-mail: gongxl@ustc.edu.cn

Z. Zhang · Z. Feng
Aerospace Research Institute of Material and Processing Technology, Beijing 100076, China

fiber bundles splitting on the net cross section [6, 12, 14]. Moreover, the conflicts widely existed in the 2D-C/Cs, while few reports were documented on the notch effects for the 3D-C/Cs. One available work in the literatures was the investigation on the comparison of fracture resistance of 2D- and 3D-C/Cs [6]. Their results indicated that the 3D-C/Cs had much higher fracture resistance than 2D-C/Cs. It was found that the net fracture stress of 3D-C/Cs was dependent on the notch depth. However, only one notch pattern was examined in their study and the notched fracture behavior was not discussed. To solve these problems, a full-field measurement is needed to analyze the notch effects of 3D-C/Cs, because it can give not only the globe tensile behavior (load-displacement curves) but also the local mechanical performances such as stress concentration, damages, and fracture behavior. However, few full-field investigations were carried out on the notch effects of 3D-C/Cs in the literatures.

Full-field measurement digital image correlation (DIC) technique has been widely applied in solid mechanics [15]. The DIC has many advantages, such as white light illumination, relative simplicity of the sample preparation, no sensitivity to the vibration, and sufficient accuracy of the measurements. Due to its excellent convenience and effectiveness, the DIC method has been increasingly applied to measure the displacements and strains of the 2D and 3D composite materials [16–18]. In this study, the DIC method was used as a full-field measurement to study notch effects of 3D-C/Cs. Both the local mechanical properties such as stress concentration, shear damage, and fracture behavior and the globe properties such as notch sensitivity and tensile behavior were analyzed and discussed.

Experiments

Materials and specimens

The 3D orthogonal C/C composite, in which the fiber bundles in three material directions are mutually orthogonal, is used in this study. The composites are composed of lots of periodic units. The in-plane unit cell size is 2.0×2.0 mm^2 and ply thickness is $\sim$0.25 mm. The test specimens are cut from the material plane 1–2. Six kinds of specimens with different notch patterns are prepared, including one hole H-I, two holes H-II-0 and H-II-90, three holes H-III, double edge notches DEN-U and -V. The purpose of these tests is to investigate the effect of different notch patterns on the notched strength. The specimen geometry and notch patterns are shown in Fig. 1. The length, width, and thickness of the specimen are 140, 25, and 3 mm. The holes and notches are drilled by wire-electrode cutting. For DEN-U and -V the radius is $\sim$90 μm in the notch root. The Aluminum tabs are used to avoid premature failure in the griping regions, whose length and thickness are 30 and 2 mm. The tests are carried out on MTS 809 testing machine with a 25kN load sensor. The speed of the crosshead is 0.05 mm per min.

Full-field measurement technique

The DIC is used as the deformation measurement, as it can obtain both the global and local deformation information of the specimen. The main idea of the DIC method is to correlate the two surface feature images of object before and after deformation, and then the displacement of any point on the specimen can be calculated by correlation algorithm. Displacement accuracy can reach 1 μm. More details of DIC method can be found in the review [15]. In this study, the sub-pixel search method is Newton–Raphson [19], the step size is 5×5 pixels, and the sub-image size is 25×25–45×45 pixels. To smooth the displacement field and obtain the accurate strain field, a local quadratic fitting data technique is used. The smoothing window is 5×5–9×9. The experimental images are acquired by a CCD camera and the image sampling rate is 1 picture per second. The image gray-level is 256 and the resolution is 1624×1236 pixels. Two different magnification telecentric lenses are used to obtain globe and local deformation. Before the experiment, the random speckles are sprayed on the specimen surface with the white and black paint.

Results and discussions

Dependence of strain distribution and stress concentration on material heterogeneity

Due to the geometry discontinuity, the stress concentration arises in the root of the notches or holes. Stress concentration factor (SCF, K) is used to define the degree of local maximum stress relative to the applied loading. However, the measurement of stress in the experiment is difficult, thus the stress analysis was always substituted by the strain analysis in the experiment. Using the Hooke's law, the stress can be calculated based on the strain measurement. Figure 2a shows the typical strain mapping under the load value of 60 MPa. In order to illustrate the relationship between the strain distribution and the fiber bundles architecture, the fiber bundles in 1 and 2 direction are plotted in the mapping as the solid lines and dash lines, respectively. It is found that the fiber bundles in the vicinity of the hole strongly influence the strain distribution. The strain concentration locations do not appear at the hole tips (the $\pm 90°$ locations with respect to the loading direction), while the locations shift away from the hole tips. However,

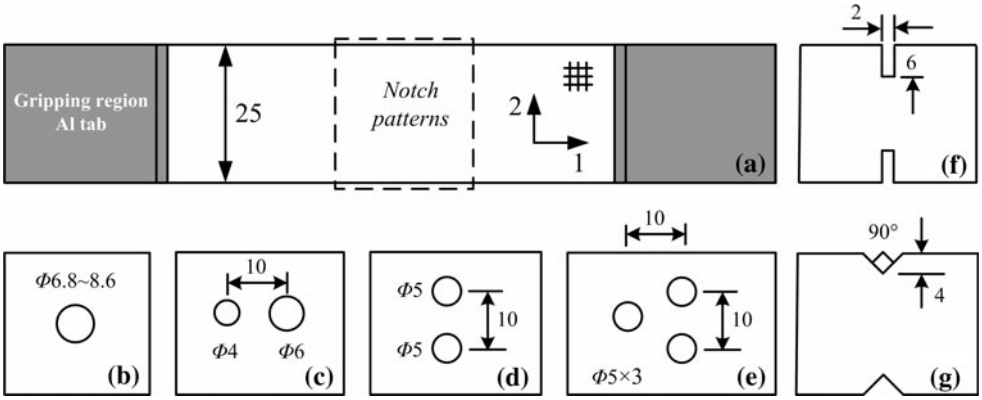

Fig. 1 Specimen geometry: (**a**) and notch patterns **b** H-I, **c** H-II-0, **d** H-II-90, **e** H-III, **f** DEN-U, **g** DEN-V

the strain concentrates can be observed at the hole tips in the homogenous materials.

Figure 2b–f show the shear strain distribution with different notch patterns. All the results indicate that the narrow shear zones (called as shear bands [2]) exist at the notch root. The period strain fluctuation in the shear bands is dependent on the local fiber bundles architecture. Due to the low shear stiffness and strength of 3D-C/Cs, shear damages are expected to exist at the notch root along the loading direction. However, these damages are difficult to be observed in the fractured specimens after the loading stage, because the damages (cracks) are closed after removing the applied loading. Moreover, initial cracks or splitting are easily induced during the cooling stage from the processing temperatures [6, 20]. It is difficult to distinguish the loading cracks from the initial defects. In this study, the DIC is used to monitor shear bands during the loading stage. Although it is difficult to observe the microcracks using the DIC, the large shear strain can also indicate the existence of the damages. As shown in Fig. 2b–f, all results reveal that the shear bands occur at the notch tips.

Figure 3 shows the typical strain concentration with different fiber meso-structures in the vicinity of the hole. Because of the strain fluctuation within a unit cell, the concentrated strain is averaged on a unit cell region (2×2 mm^2) at the hole tip (90° locations with respect to the loading direction). The average strain should represent the macro tensile behavior of the materials at the hole tip. Since the strain ε_2 can be neglected, the concentrated stress is proportional to the concentrated strain ε_1 (Hooke's law). Therefore, the slope of the curves, K, is almost equal to the SCF. The meso-structure-1 and -2 are two typical meso-strucutres at the hole tip. As shown in Fig. 3, the SCF of meso-structure-1 is 46 % higher than that of meso-structure-2. That means the SCF is greatly dependent on the meso-structures in the vicinity of the hole. Furthermore, the results indicate the SCF of 3D-C/Cs is much lower than that of homogeneous materials. This fact may be related to the shear deformation of the 3D fiber bundle structures.

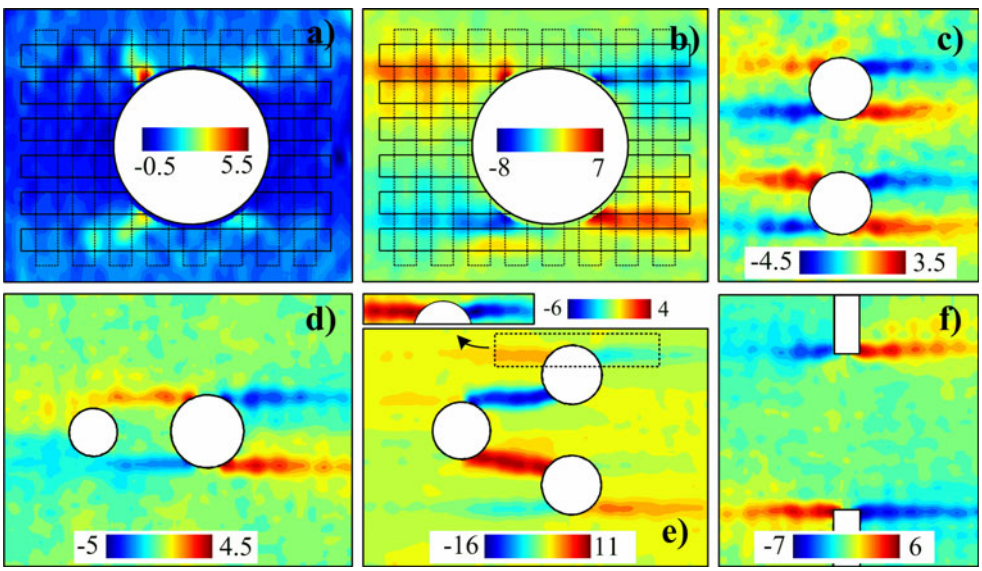

Fig. 2 Strain contours under 60 MPa: **a**, **b** are the normal and shear strain of one hole case, **c**, **d** are the shear strain of two holes case, **e** shear strain of three holes case, **f** shear strain of DEN-U case (1000 με)

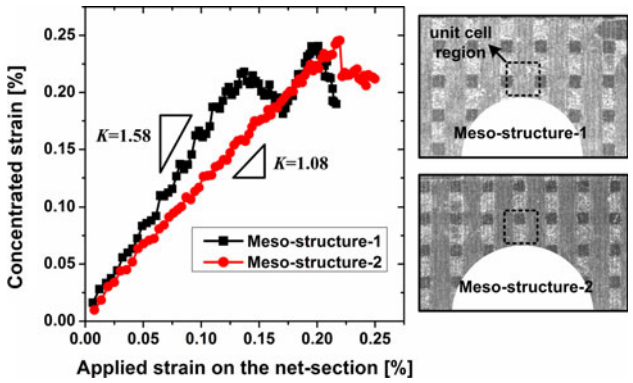

Fig. 3 Stress concentration under different fiber meso-structures in the vicinity of the hole

Notch sensitivity under different notch patterns

Generally, the effect of notches (holes) on the ultimate load of specimen can be divided into two aspects. First, the notches reduce the cross section area that lowers the applied load. Second, the stress concentration introduced by the notches makes the stress at the notch root high enough to destroy the specimen even though the applied load is relatively low. To evaluate the effect of stress concentration on the ultimate load of the notched specimen, the notch strength ratio (NSR) [21] is defined as $\mathrm{NSR} = \frac{\sigma^n_{\mathrm{net}}}{\sigma^n}$, where σ^n is the unnotched strength, σ^n_{net} is the net strength (notched strength). The net strength σ^n_{net} is the average fracture stress on the net cross section, which can be expressed as $\sigma^n_{\mathrm{net}} = \frac{P}{(W-h)t}$, where P is the ultimate load, and W, h, and t are the width, notch depth, and thickness of the specimen, respectively. Using the NSR index, the effect of the notches on the tensile strength of the engineering materials can be classified into three kinds [22]: notch strengthening materials when $\mathrm{NSR} > 1$, notch weakening materials when $\mathrm{NSR} < 1$, and notch insensitivity materials when $\mathrm{NSR} = 1$.

The influence of notch patterns on the NSR is shown in Fig. 4. It is found that the NSR is close to 1 under different notch patterns. For H-I, five specimens with different meso-structures in the vicinity of the hole are tested. The results indicate that the influence of the meso-structures on the net strength is not strong. As discussed in "Dependence of strain distribution and stress concentration on material heterogeneity" section, the SCF is highly dependent on the meso-structures; which shows that the notch sensitivity is not greatly dependent on the SCF. Although the material heterogeneity influences the concentrated stress at the notch root, it slightly affects the net fracture stress before specimen failure. As shown in Fig. 3, the concentrated strain does not increase linearly with the applied strain. Before the final fracture occurs, both of the concentrated strains come to the range between 0.2 and 0.25 % which is in the range of unnotched fracture strain. This result indicates that the stress redistribution mechanism may exist to make the stress on the net cross section uniform before specimen failure. As shown in Fig. 2b, the shear bands are expected to be the mechanism to diffuse the stress concentration. Similar phenomenon has also been found in CMCs [2].

In comparison to one hole case, the stress of multi-holes cases (H-II and H-III) should be under multiaxial stress states due to the interaction of holes. However, this stress interaction does not affect the notch sensitivity, which means the constant net strength rule is not broken by the presence of multi-holes. It should be noted the net area to bear the loading in the H-III case is slightly different with other cases. As shown in Fig. 5, the net cross section in H-III consists of tensile surface and shearing surface. Thus the ultimate load can be expressed as tension force plus shearing force. For the DEN-U and -V cases, the fact that the net strength is not influenced by the notches patterns can also be verified. The radius of curvature is only 90 μm in notch root of DEN-U and -V specimens. Based on the elastic theory, the stress concentration should be very high at the notch root. However, this sharp corner shows few influence on the net strength σ^n_{net}. All the tests indicate that the fracture stress on the net cross section is constant and it is not influenced by the notch patterns.

The influence of the notch depth on the notch sensitivity is also not strong. As shown in Fig. 4, notch depth to width ratio is varied from 16 to 58 %. However, the net strength is almost the same (NSR = 1). The notch insensitivity means the structure strength is only dependent on the net cross section area. Thus, residual load can be easily calculated using the minimum net cross section area to multiply by the unnotched strength.

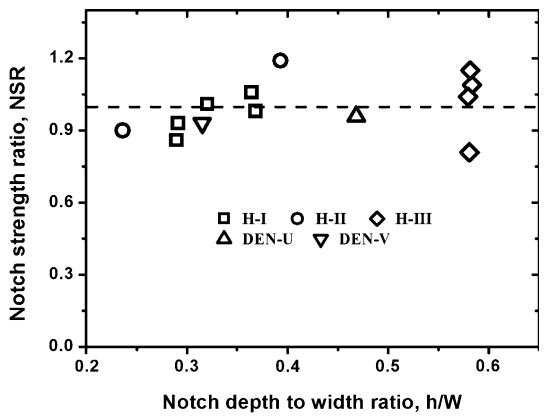

Fig. 4 Influence of notch patterns and notch depth on the notch strength ratio (NSR)

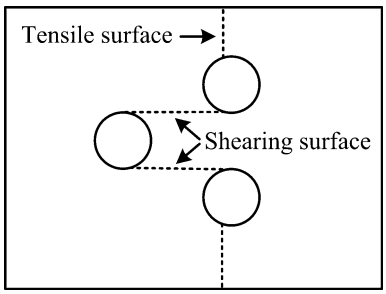

Fig. 5 Net cross section illustration of the three holes case

Full-field analysis of the fracture behavior

As shown in Fig. 6a, the fibers pull-out is found on the surface of fractured specimen. However, sequent images monitored by the CCD camera show the fibers pull-out just occasionally occurs at the final fracture moment. Figure 6b shows the fracture behavior before specimen failure. Little visible fiber bundles failure can be observed in the net section regions. In the experiment the total loading time is 16 min. The image sampling rate is 1 picture per second. Thus, the fracture behavior exhibits the catastrophic brittle fracture.

In order to get a better understanding of the fracture behavior on the net cross section region, we calculate the strain distribution in the dash line box in Fig. 6b by the DIC method. It should be noted that if there exists geometry discontinuity caused by fiber bundles fracture or splitting, the speckle patterns will be de-correlated and the DIC method will fail to obtain the accurate displacement. The displacement error can lead the measured strain on the discontinuity regions extremely high (larger than 0.01). Therefore, by judging the maximum strain, the strain mapping can still be used as an index to reveal whether the discontinuity exists. Figure 6c–e show the strain distribution ε_1, ε_2, and γ_{12} in the front of notch tip, where the dash line is the position between the two notches. The results show that the strain ε_1 is in the range of 1500–3000 με, the strain ε_2 is $\sim$600–1400 με, and the shear strain γ_{12} is ~ -1000–1500 με. The strain fluctuation in the test region should be related to the material heterogeneity. It is found that the strain ε_2 and γ_{12} are quite lower than the strain limit, which indicates that no obvious fiber bundles failure or splitting on the net cross section exists. The average strain ε_1 in the test region is 2400 με, which is also in the range of unnotched tensile strain limit (2000–3000 με). Furthermore, the large concentrated strain is not found near the notch root; which indicates the stress concentration has been vanished before specimen failure. The normal stress on the net cross section should be uniform before the final fracture.

Figure 7 shows the typical fracture behavior. The fracture occurs at the notch root where the cross area is minimum. The fibers pull-out is observed on the fracture surface of the specimens. It can be found that the long pull-out fiber bundles are only found outside of the specimen.

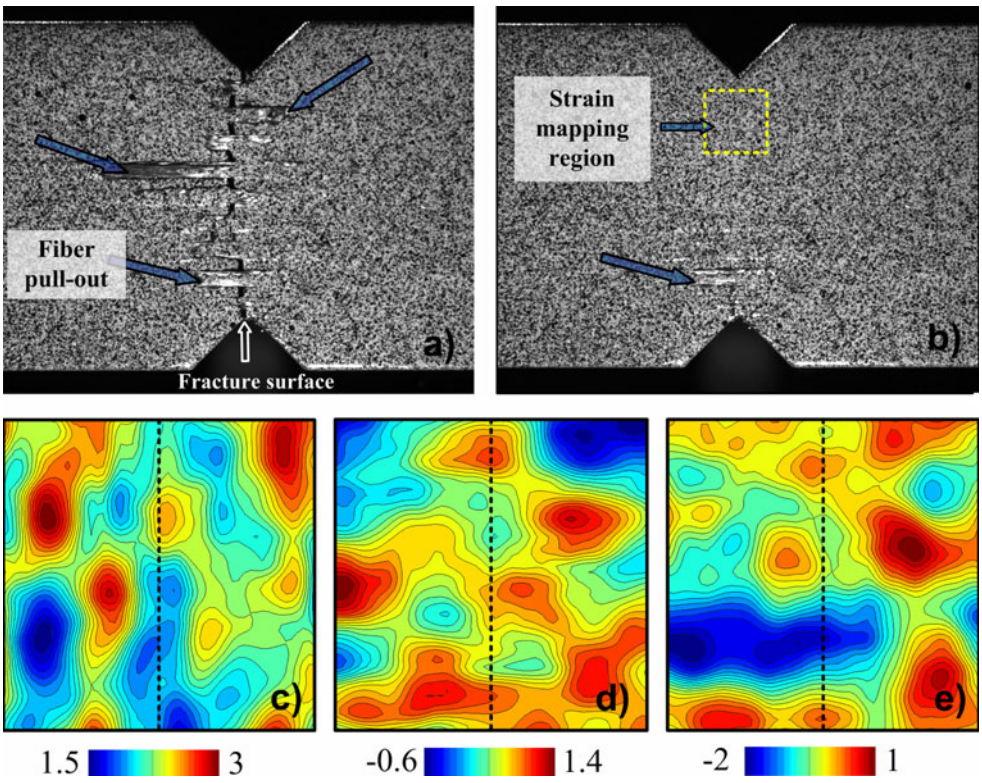

Fig. 6 Fracture behavior and strain distribution on the net cross section: **a** after failure, **b** before failure, **c–e** are strain contour ε_1, ε_2, and γ_{12} in the strain mapping region (1000 με)

Inside of the specimen, the fibers pull-out is short and fracture surface is relatively flat. The fibers pull-out length near the notch root has no distinct differences with that far away from the notch root. Based on the above analysis, it can be deduced that the stress on the net cross section should be constant.

Influence of shear damages on the tensile behavior

The tensile response is discussed in this section. The relative displacement of the gauge length is measured by the DIC method. The gauge length is 20 mm. Due to the presence of the notches (holes), the displacement in the width direction of the specimen is not uniform. The apparent displacement in the Fig. 8 is the average displacement on the width direction, which represents the globe tensile deformation of the specimen. The net displacement is the deformation on the net section region, which characterizes the tensile behavior on the net section. For specimen H-I, the net displacement is the elongation of the edge line of the specimen. For specimen DEN-V, the net displacement is the elongation of the central line of the specimen. The net displacement is used to investigate whether the notches affect the tensile behavior on the net section.

The pictures of shear damages evolution in Fig. 8 are obtained based on the full-field measurements. First, the full-field shear strain mapping is measured by DIC method. Then, the binaryzation image of the mapping is obtained through adaptive threshold segmentation, where the strain lower than 0.01 is set to 0 (blue regions) and the strain larger than 0.01 is set to 1 (red regions). Based on our previous study [23], the in-plane shear strain limit of 3D-C/Cs is ~0.01. Thus, the red regions are considered as the damage zone.

Figure 8 shows the typical load–displacement curves (σ–s). From the apparent σ–s curve, it is shown that tensile

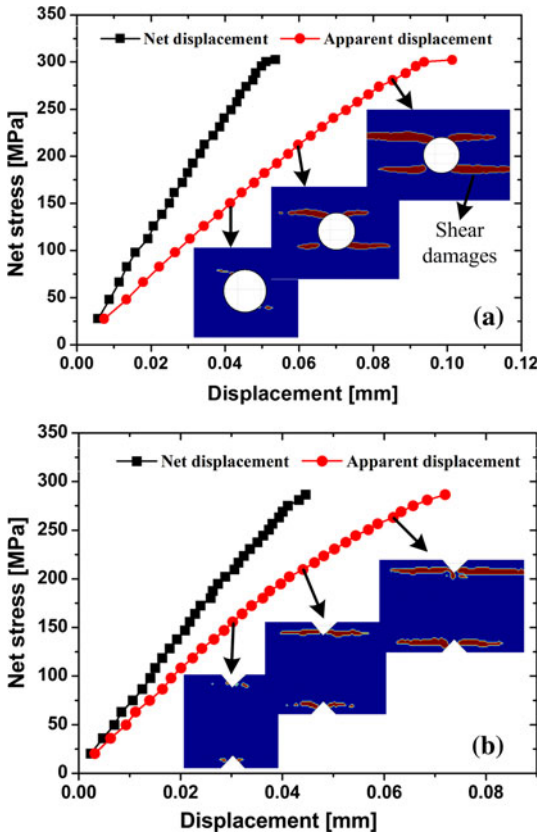

Fig. 8 Load-displacement curves and shear damage evolution: **a** specimen H-I, **b** specimen DEN-V

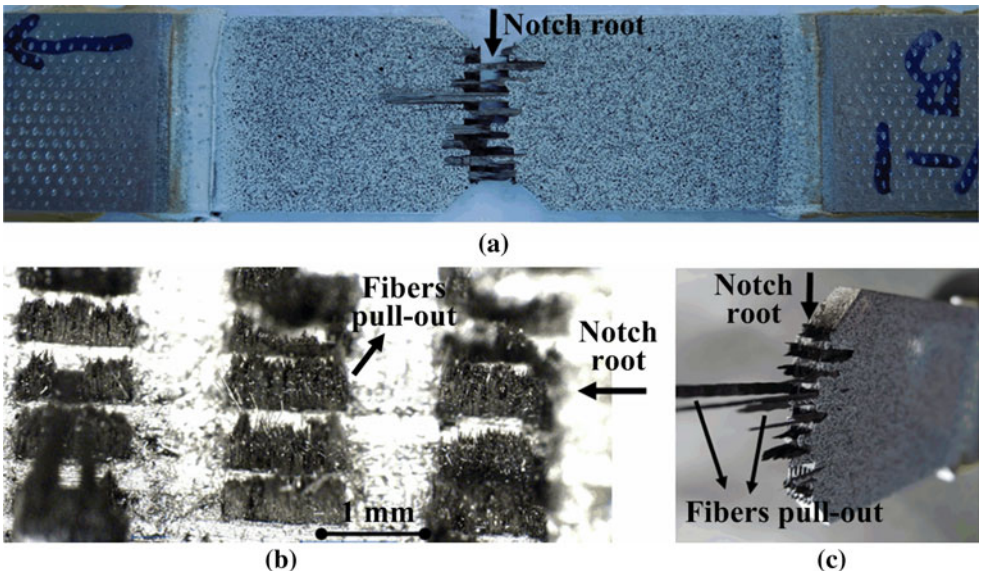

Fig. 7 The typical fracture morphology: **a** globe fracture, **b** fibers pull-out outside of specimen, **c** fibers pull-out inside of fracture plane

behavior of notched specimen exhibits a nonlinear characteristic and the stiffness of notched specimen decreases gradually. It is found that the nonlinearity is caused by the growth of the shear damages. As shown in Fig. 8, when shear damages occur, the apparent σ–s curve begins to exhibit nonlinearity. With extending of the damaged regions, the degree of nonlinearity increases. However, the net σ–s curve is still linear which is similar with the tensile behavior of the unnotched specimen; which reveals that the presence of notches does not affect the tensile behavior on the net cross section. Due to the low shear strength of 3D-C/Cs, the shear bands cannot transmit enough large shear stress to affect tensile behavior of the net section. Finally, the net section region can be considered as unnotched specimen under uniaxial tensile load. The elongation, δ, on the net cross section is also similar with the unnotched results. For H-I case, elongation $\delta = 0.26$ %; for DEN case, $\delta = 0.23$ %, both of them are in the unnotched elongation range between 0.2 and 0.3 %.

Conclusions

In this study, the notch effects of 3D C/Cs were investigated with different notch patterns by DIC method. Based on the experiment data, several conclusions were obtained.

1) For 3D-C/Cs, the stress concentration was different from that of homogeneous materials. First, the mesostructures in the notch root greatly affect the SCF. For another, the SCF was much lower than the results of the homogeneous materials.
2) The NSR was approximately equal to 1, which was independent on the material heterogeneity, notch patterns, and notches depth. Thus, the ultimate loading of a notched specimen could be simply predicted using the minimum cross section area to multiply by the material strength.
3) The full-field strain mapping revealed that there were no large inelastic normal and shear strain on the net cross section. The stress on the net cross section should be uniform before the final fracture.
4) The tensile behaviors of the net cross section, such as linear σ–s relation, catastrophic brittle fracture, and the elongation, were not influenced by the presence of notches.

Acknowledgements Financial support from the National Natural Science Foundation of China (Grant No. 11125210) is gratefully acknowledged.

References

1. Cady CM, Mackin TJ, Evans AG (1995) J Am Ceram Soc 78:77
2. Mackin TJ, Purcell TE, He MY, Evans AG (1995) J Am Ceram Soc 78:1719
3. Mackin TJ, Perry KE, Epstein JS, Cady C, Evans AG (1996) J Am Ceram Soc 79:65
4. Mattoni MA, Zok FW (2004) J Am Ceram Soc 87:914
5. Haque A, Ahmed L, Ramasetty A (2005) J Am Ceram Soc 88:2195
6. Aly-Hassan MS, Hatta H, Wakayama S, Watanabe M, Miyagawa K (2003) Carbon 41:1069
7. Chen ZK, Xiong X, Li GD, Wang YL (2010) J Mater Sci 45:3477. doi:10.1007/s10853-010-4376-9
8. He YG, Li KZ, Li HJ, Wei JF, Fu QG, Zhang DS (2010) J Mater Sci 45:1432. doi:10.1007/s10853-009-4089-0
9. Ozcan S, Tezcan J, Gurung B, Filip P (2011) J Mater Sci 46:38. doi:10.1007/s10853-010-4793-9
10. Hatta H, Kogo Y, Asano H, Kawada H (1999) JSME Int J A Solid M 42:265
11. Kostopoulos V, Pappas YZ (1998) Mater Sci Eng A 250:320
12. Goto K, Hatta H, Takahashi H, Kawada H (2001) J Am Ceram Soc 84:1327
13. Griesheim GE, Pollock PB, Yen SC (1993) J Am Ceram Soc 76:944
14. Hatta H, Denk L, Watanabe T, Shiota I, Aly-Hassan MS (2004) J Compos Mater 38:1479
15. Pan B, Qian KM, Xie HM, Asundi A (2009) Meas Sci Technol 20:062001
16. Nicoletto G, Anzelotti G, Riva E (2008) Compos A 39:1294
17. Ivanov D, Ivanov S, Lomov S, Verpoest I (2009) Opt Laser Eng 47:360
18. Yang QD, Rugg KL, Cox BN, Marshall DB (2005) J Am Ceram Soc 88:719
19. Bruck HA, Mcneill SR, Sutton MA, Peters WH (1989) Exp Mech 29:261
20. Li HJ, Li HL, Li KZ, Wang YJ, Zhang DS, Lu JH (2011) J Mater Sci 46:4667. doi:10.1007/s10853-011-5373-3
21. Cui C, Demura M, Hasegawa K, Ohashi T, Kishida K, Hirano T (2005) Scr Mater 53:1339
22. Qu RT, Calin M, Eckert J, Zhang ZF (2012) Scr Mater 66:733
23. Qin LJ, Gong XL et al (2012) Compos Part A 43:310